Pt Nanocrystals: Shape Control and Langmuir−Blodgett Monolayer Formation

Hyunjoon Song, Franklin Kim, Stephen Connor, Gabor A. Somorjai, and Peidong Yang*

Department of Chemistry, University of California, Berkeley, Materials Science Division, Lawrence Berkeley National Laboratory, Berkeley, California 94720

We report the synthesis of monodisperse Pt nanocrystals with three different shapes—cubes, cuboctahedra, and octahedra, selectively, with similar sizes of 9−10 nm by a modified polyol process. We found that addition of silver ion enhances the crystal growth rate along ⟨100⟩, and essentially determines the shape and surface structure of the Pt nanocrystals. After the reaction, the silver species can be easily removed by repetitive precipitation giving pure Pt nanoparticles. Two-dimensional arrays of the Pt nanocrystals were assembled by using the Langmuir−Blodgett (LB) method. The particles were evenly distributed on the entire substrate, and their surface coverage and density can be precisely controlled by tuning the surface pressure. The resulting Pt LB layers are potential candidates for 2-D model catalysts as a result of their high surface area and the structural uniformity of the metal nanocrystals.

Introduction

Metal nanocrystals with precisely controlled shape exhibit unique optical, magnetic, and catalytic properties.[1] There have been extensive studies on approaches to control size and shape of the metal nanoparticles, and most of the methods developed thus far can be categorized as either reduction or decomposition of the metal precursors in the presence of organic capping reagents in solution. Cetyltrimethylammonium bromide (CTAB) and poly(vinylpyrrolidone) (PVP) have been widely used as regulating agents for the selective growth of nanocrystals with well-defined shapes such as rods,[2,3] prisms,[4] and cubes.[5] Recently, Yang et al. reported the synthesis of gold nanocrystals with various shapes by refluxing gold precursor in ethylene glycol (EG) in the presence of PVP.[6] Murphy et al. have also prepared a variety of gold colloids from the cubes to the branched particles on the basis of seed-mediated growth with CTAB.[7] However, the exact binding nature between these capping reagents and the specific crystallographic planes is still elusive, and there are no generalized mechanisms interpreting various metal nanocrystal shape-control experiments.

Since El-Sayed and co-workers reported the Pt cube synthesis using polymer capping agents,[8] many researchers tried to make various shapes of the Pt particles[9] in order to investigate their influence on catalytic activity.[10] El-Sayed et al. have synthesized three different shapes of the Pt nanocrystals and have run the electron-transfer reaction between hexacyanoferrate(III) and thiosulfate ions.[11] While this study gives intriguing correlations between the kinetic parameters of the reaction and surface atom fraction in each shape, more uniform Pt nanoparticles in terms of the size and shape are required to precisely quantify the catalytic influences. Herein we report the synthesis of monodisperse Pt nanocrystals with various shapes—cubes, cuboctahedra, and octahedra, selectively, in the same range of the particle size (9−10 nm). We found that silver ion enhances the crystal growth rate along ⟨100⟩, and essentially determines the shape and surface structure of the Pt nanocrystals. This process may be applicable to other metal and semiconductor nanostructures, and may provide insights for a general mechanism on

morphology control of nanocrystals. We also demonstrated two-dimensional organization of the Pt nanocrystals by the Langmuir−Blodgett (LB) technique. The resulting Pt layer structures will be exploited as ideal 2-D model catalysts as a result of their high surface area, the tunable interparticle spacing, and the structural uniformity of the metal nanocrystals.

Experimental Section

Materials. Dihydrogen hexachloroplatinate ($H_2PtCl_6 \cdot 6H_2O$, 99.9%, metals basis) was purchased from Alfa Aesar. Silver nitrate ($AgNO_3$, 99+%) and poly(vinylpyrrolidone) (PVP, M_w = 55 000) were obtained from Sigma-Aldrich. Ethylene glycol (EG) and all other solvents were of analytical grade and were used without further purification.

Synthesis of Pt Nanocrystals. A volume of 2.5 mL of EG was refluxed for 5 min. Then, 93.8 μL of 0.375 M PVP (total 3 mL, PVP/Pt salt = 12:1) and 46.9 μL of 0.0625 M $H_2PtCl_6 \cdot 6H_2O$ (total 1.5 mL) solutions in EG were added to the boiling EG every 30 s over a 16-min period. The resulting mixture was refluxed for an additional 5 min. The product was centrifuged at 5000 rpm for 15 min. The supernatant was separated and precipitated by adding a triple volume of acetone, followed by centrifugation at 3000 rpm for 5 min. The precipitate was collected and redispersed in 3 mL of ethanol with sonication. A volume of 9 mL of hexane was added to the dispersion, and the solution was centrifuged at 3000 rpm for 5 min. The precipitate was washed twice with the same solvent mixture. Finally, the precipitate was dispersed in 3 mL of ethanol.

For Pt cube synthesis, 0.5 mL of 2×10^{-3} M $AgNO_3$ solution in EG (Ag salt/Pt salt = 1.1 mol %) was added to the boiling EG prior to the addition of PVP and Pt precursors. For Pt cuboctahedron and octahedron samples, 0.5 mL of 2×10^{-2} M (Ag/Pt = 11 mol %) and 6×10^{-2} M (Ag/Pt = 32 mol %) $AgNO_3$ solutions in EG were added to the boiling EG, respectively. PVP and Pt salt solutions were immediately added to the reaction mixture.

For mechanism studies, several aliquots of the reaction mixture were collected in an appropriate time during the reaction, and checked by UV−Vis spectroscopy.

* Corresponding author. E-mail: p_yang@uclink.berkeley.edu.

Pt Nanocrystals: Shape and Surface Structure

J. Phys. Chem. B, Vol. 109, No. 1, 2005 **189**
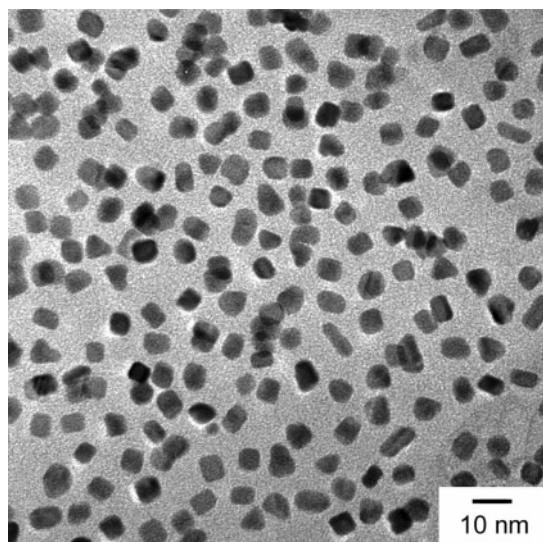
Figure 1. TEM image of the Pt nanocrystals synthesized without AgNO₃ addition.
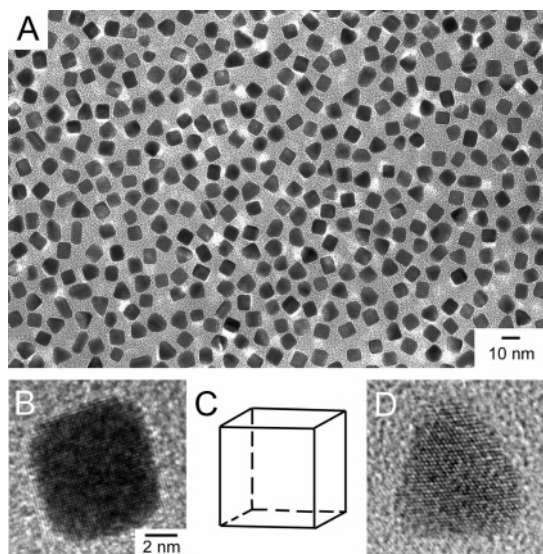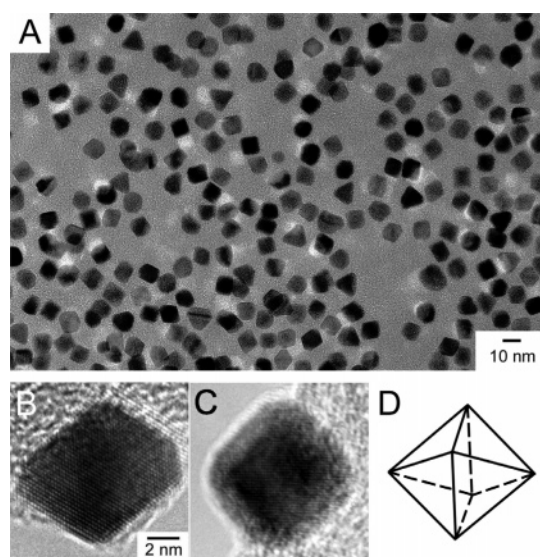

Figure 2. (A) TEM image of the Pt cubes. (B) HRTEM image of the Pt cube along the [001] zone axis. (C) An ideal cube structure. (D) HRTEM image of the Pt tetrahedron along the [111] zone axis.

Langmuir−Blodgett Layer Formation. The Pt colloidal solution in ethanol was precipitated by adding a triple volume of hexane. The precipitate was redispersed in 3 mL of chloroform with sonication. LB experiments were done with deionized water on a LB trough (Nima Technology, M611) at room temperature. The surface pressure was monitored with a Wilhelmy plate, and was adjusted to zero before spreading the particles. The chloroform solution of Pt cubes was slowly spread on the water surface of the trough. The resulting surface layer was compressed by moving the mobile barrier at a rate of 15 cm²/min. At the different stages of compression, the Pt layers at the water−air interface were carefully transferred onto continuous carbon TEM grids using the Langmuir−Schäffer horizontal liftoff method.

Characterization. Transmission electron microscopy (TEM), high-resolution transmission microscopy (HRTEM), and energy-dispersive X-ray spectroscopy (EDX) experiments were made on a Philips CM200 microscope operated at 200 kV at the National Center for Electron Microscopy at Lawrence Berkeley National Laboratory. The Pt colloidal solutions in EG were deposited on carbon-film-coated copper grids (Ted Pella). X-ray
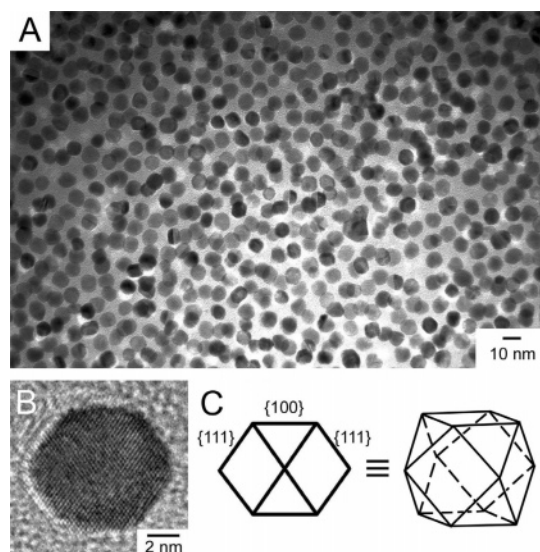
Figure 3. (A) TEM image of the Pt cuboctahedra. (B) HRTEM image of the Pt cuboctahedron along the [110] zone axis. (C) An ideal cuboctahedron structure and its 2-D projection along the [110] direction.

Figure 4. (A) TEM image of the Pt octahedra. (B) HRTEM image of the Pt octahedron along the [110] zone axis. (C) HRTEM image of the Pt octahedron along the [001] zone axis. (D) An ideal octahedron structure.

**TABLE 1: Yield and Average Size of the Pt Nanocrystals**

amount of Ag added[a]	major shape yield, average size	minor shape yield, average size
1.1 mol %	cubes ∼80%, 9.4 ± 0.6 nm	tetrahedra ∼10%, 9.8 ± 0.7 nm
11 mol %	cuboctahedra ∼100%, 9.1 ± 0.6 nm	
32 mol %	octahedra ∼80%, 9.8 ± 0.6 nm	tetrahedra ∼10%, 9.9 ± 0.7 nm

[a] With respect to the Pt salt concentration.

diffraction (XRD) patterns were measured on a Bruker D8 GADDS diffractometer using Co Kα radiation (1.79 Å). UV−Vis absorption spectroscopy experiments were carried out on an Agilent 8453 UV−Vis system.
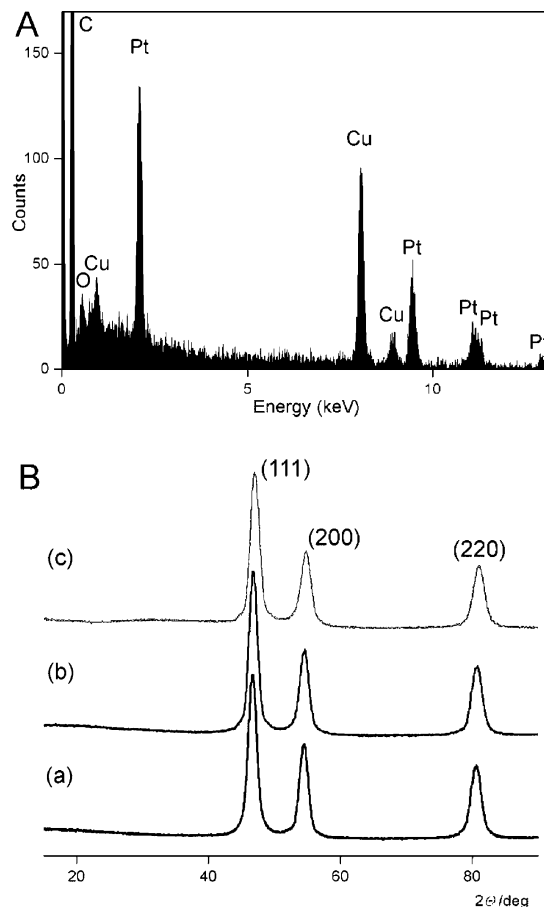
Results and Discussion

Synthesis and Morphology Control of Pt Nanocrystals. In a typical synthesis, EG solutions of PVP (93.8 μL of 0.375
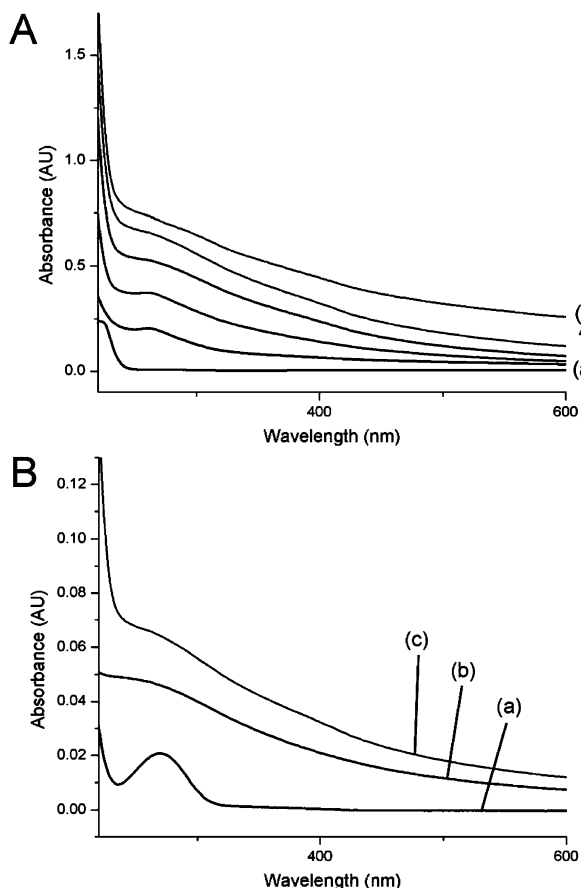
Figure 5. (A) UV−Vis absorption spectra of the Pt octahedron sample during the reaction. The aliquots were collected (a) 0, (b) 0.5, (c) 5, (d) 16, (e) 21, and (f) 76 min after the addition of AgNO₃. (B) UV−Vis spectra of (a) the supernatant after the second centrifugation in EG, (b) the purified Pt octahedra, and (c) as-prepared mixture without purification.


Figure 6. (A) EDX spectrum of the pure Pt octahedra. (B) XRD spectra of (a) the cubes, (b) the cuboctahedra, and (c) the octahedra.

M) and dihydrogen hexachloroplatinate (46.9 μL of 0.0625 M) were added to the boiling EG every 30 s over a 16-min period. EG serves both as a solvent for dissolving the reactants and as a reducing agent. The color of the solution immediately changed from yellow to dark brown, indicating the fast reduction of Pt-(IV) to Pt(0) species. The solution was refluxed for an additional 5 min. Without adding Ag ions, the particles were obtained as a mixture of different shapes. Figure 1 exhibits various shapes of the Pt particles synthesized in this reaction including cubes with round edges (∼40%), tetrahedra (∼10%), spheres and facets (∼30%), and irregular rods (∼20%). However, when 1.1 mol % of AgNO₃ (with respect to the Pt concentration) was introduced into the solution, Pt cubes (∼80%) were preferentially obtained with a small amount of tetrahedra (∼10%) after purification. A TEM image (Figure 2A) shows that the Pt cubes are homogeneous in shape with a narrow size distribution (face-to-face: 7.1 ± 0.6 nm, vertex-to-vertex: 9.4 ± 0.6 nm). An HRTEM image (Figure 2B) of a Pt cube demonstrates the exposed {100} surface of the cube oriented along the [001] zone axis. The distance between the adjacent lattice fringes is 1.96 Å, in good agreement with the interplanar distance of the (200) plain in the face-centered cubic (fcc) Pt structure. The minor tetrahedral particles are in the average size of 9.8 ± 0.7 nm. Figure 2D shows a triangular projection of the tetrahedral particles along the [111] direction, in which all side faces are covered with {111} planes.

Increasing the AgNO₃ concentration to 11 mol % changes the morphology of the Pt particles. Faceted particles were mostly

obtained (∼100%), including hexagons as the majority after purification (Figure 3A). The Pt nanocrystals are monodisperse with the largest vertex-to-vertex distance of 9.1 ± 0.6 nm. Figure 3B is a representative HRTEM image of the hexagon, and clearly shows the lattice fringe image of {111} planes with the interplanar distance of 2.26 Å and the separation angle of 70°, consistent with the hexagonal projection of an ideal cuboctahedron along the [110] zone axis (Figure 3C). In this projection, four {111} and two {100} facets are placed on the edges of the hexagonal shape. Other facets represent the projections from the cuboctahedral structure along different orientations.

At higher concentrations of AgNO₃ up to 32 mol %, the resulting Pt nanocrystals are dominated by diamond- and square-shaped particles (∼80%) with tetrahedra (∼10%) (Figure 4A). The average vertex-to-vertex distance of the major particles is 9.8 ± 0.6 nm. Figure 4B shows HRTEM image of a diamond-shaped particle, which turns out to be the [110] oriented Pt octahedron. The two ends of the octahedron are slightly truncated. The square shapes are not from the Pt cubes, but from the same octahedra oriented along the [001] zone axis.[12] Figure 4C exhibits four {111} facets edged on the Pt octahedron, while four {100} planes are located on the edges of a Pt cube along the same direction. The ideal model of the octahedron (Figure 4D) indicates that the surface is covered with {111} faces.

All three Pt particles were carefully purified by repetitive centrifugation and dispersion. Table 1 shows that all particles generated in this reaction were in the similar sizes of 9−10 nm with narrow distributions less than $\sigma \sim 7\%$. It means that the shape is the decisive factor for the surface structure of each nanocrystal. Considering the ideal models, the cube has {100}

Pt Nanocrystals: Shape and Surface Structure

J. Phys. Chem. B, Vol. 109, No. 1, 2005 **191**
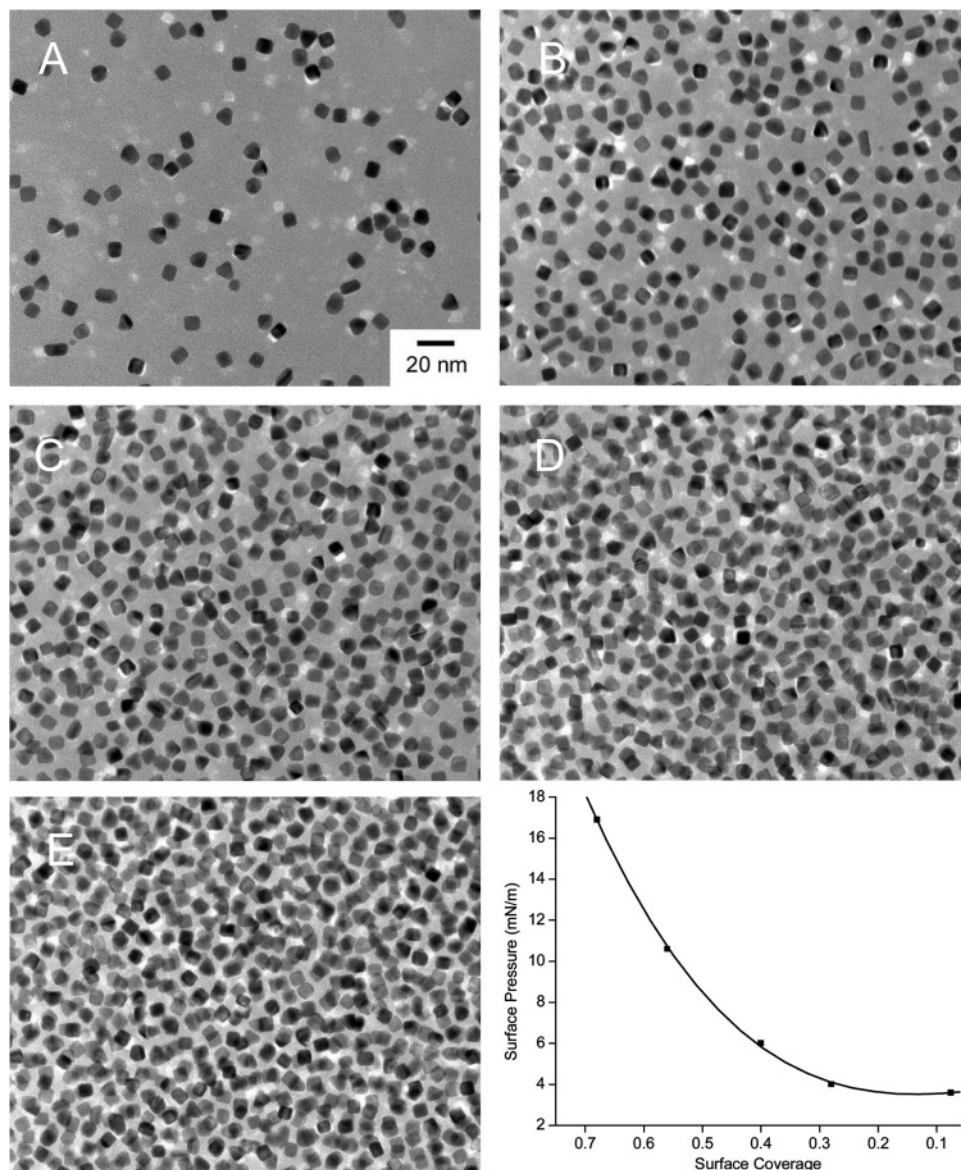
Figure 7. LB layers of the Pt cubes deposited at the surface pressure of (A) 3.6 mN/m, (B) 4.0 mN/m, (C) 6.0 mN/m, (D) 10.6 mN/m, and (E) 16.9 mN/m. (F) Pt cube nanocrystal coverage (estimated from TEM data) as a function of the surface pressure during the LB process.

faces (Figure 1C), and the octahedron and tetrahedron display {111} surfaces (Figure 4D). In the cuboctahedron, the surface is composed of six {100} and eight {111} planes with an area ratio of 1:0.577 (Figure 3C). Accordingly, surface-dependent properties such as catalytic reactivity[13] can be modified rationally by manipulating the shape of the particles with a variation of the added silver ion. Several shapes of Pt nanoparticles have been successfully synthesized previously,[8,9] but there were few reports to tune both the size and shape of nanocrystals simultaneously under the same reaction conditions.

Addition rate of the reactants is important to control the size of Pt nanocrystals. If the PVP and Pt salts were added all at once, small and irregular Pt particles were generated with the average size less than 4 nm. On the other hand, slow addition of the PVP and Pt salt solutions over a period of 30 min led to polycrystalline particles larger than 13 nm. These experiments indicate that the particle size can be adjusted by controlling concentration of seeds formed at the early stages of the reaction.

Plausible Mechanism and Purification of Pt Nanocrystals. It is commonly believed that the final morphology of the fcc nanocrystals is dependent upon the R value, defined as the relative growth rate along the $\langle 100 \rangle$ direction with respect to

that of the $\langle 111 \rangle$.[12,14] As the concentration of Ag ion increases in the reaction mixture, the majority of the Pt particles changes from the cubes ($R = 0.58$) to the cuboctahedra ($R = 0.87$), and eventually to the octahedra ($R = 1.73$). It reveals that introduction of the Ag ion enhances the growth along $\langle 100 \rangle$, and/or suppresses the growth along $\langle 111 \rangle$. The reaction progress of Pt octahedron synthesis was monitored by UV−Vis absorption to support this mechanism. At early stages of the reaction (Figure 5A, (b) and (c)), a clear absorption band at ∼270 nm was observed. The strong absorption at 270 nm was also observed under the same reaction in the absence of the Pt salts. It is probably attributed to the reduced silver species such as Ag_4^{2+}, which is the most stable intermediate formed in the reduction of silver nitrate by γ-irradiation and sodium borohydride.[15] This silver species seems to be preferentially adsorbed on more active {100} surfaces of the Pt nuclei than {111} facets during the reaction. Strüber et al. reported that the desorption energy of Ag on the Pt(100) single crystalline surface is higher than that on Pt(111) in the Ag monolayer film growth, indicating the relative stability of Ag(0) on the Pt{100} surface.[16] When the Pt precursors were continuously added, the Pt salts were reduced spontaneously with the oxidation of adsorbed Ag species on

the {100} surface by favorable electrochemical reaction (4Ag + H$_2$PtCl$_6$ → 4AgCl + Pt(0) + 2HCl), and subsequently the growth rate along the ⟨100⟩ direction was enhanced with the dissolution of AgCl into the solvent. In Figure 5A (c)−(f), the peak at 270 nm is diminished, and the broad shoulder appears at ∼290 nm as the reaction proceeds, indicative of consumption of the reduced silver species with the concomitant formation of Pt(0) nanoparticles.

Importantly, silver byproducts can be effectively removed by repetitive precipitation. After the reaction, the product consisted of Pt particles as well as AgCl, reduced silver species, and silver particles (Figure 5B (c)). The first centrifugation precipitated AgCl as a white powder as a result of its low solubility in EG at room temperature. Adding acetone into the mixture precipitated the Pt particles by centrifugation, while the reduced silver species and free-standing PVP stayed in the supernatant as seen in Figure 5B (a), exhibiting strong absorption at 270 nm. The clean Pt particles were obtained by precipitation and redispersion in an ethanol/hexane (1:3) mixture several times, and were characterized by UV absorption, EDX, and XRD. Figure 5B (b) shows a very broad signal at ∼290 nm, but no distinguishable peaks at ∼270 nm (for reduced silver species) and ∼400 nm (for Ag particles). There were no detectable Ag signals in EDX nor in XRD spectra (Figure 6) within the detection limit. These results suggest that Ag ions may act as a shape-control reagent during the reaction, and can be easily removed to produce pure Pt particles without significant alloying between Ag and Pt. This is opposite to the Galvanic replacement reaction of Ag nanoparticles and gold salts giving the Au/Ag alloy wall structure.[17]

It is interesting to point out that previously reported gold nanorod synthesis by photochemical and electrochemical methods[3] may follow the analogous mechanism. Introducing Ag ions enhances the ⟨100⟩ directional growth, and subsequently controls the aspect ratio of the nanorods. The resulting rods contain no Ag composition in their lattice as well. We believe that this process can be applicable to other metal and semiconductor systems using various foreign ions as shape-control agents.

Langmuir−Blodgett Layer Formation of Pt Nanocrystals. The LB technique is one of the powerful tools for fabricating the monolayer of nanoscopic structures[18] such as quantum dots,[19] rods,[20] and wires[21] on various substrates. This method was utilized for 2-D organization of the Pt nanocrystals here. The Pt cubes were dispersed in chloroform, and the solution was slowly deposited on the water surface of the trough. The surface pressure increased up to 3.6 mN/m during the deposition, presumably as a result of the presence of weakly bound PVP molecules. The layers were collected frequently by TEM grids with the horizontal liftoff method in order to examine the particle distribution. Even at low surface pressure, the particles were evenly distributed on the entire area of the grids, and no particle aggregation was observed in Figure 7A. The surface coverage was estimated by counting the particles on the same area of the TEM grids. As the surface pressure increased up to 6.0 mN/m, the surface coverage rapidly changed from 7.6% to 40%. The particles formed a continuous monolayer, but they showed no long-range ordered structures as seen in Figure 7C. This is mainly attributed to the high-molecular-weight PVP coordinated on the Pt surface. Heath et al. have reported that the size of the passivating ligand plays important roles in determining the 2-D structures.[19c] When the small Au particles (∼2 nm) were capped with oleylamine (excess conical volume, V_e > 350 Å), the phase diagrams were dominated by 1-D structures at low surface pressures and 2-D formlike phases at high pressures. The close-
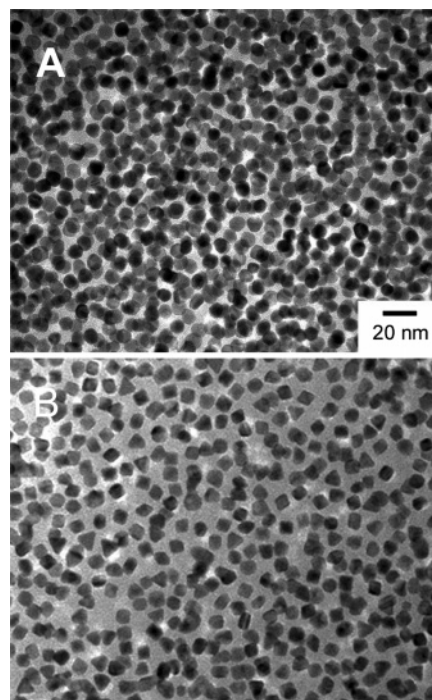
Figure 8. LB monolayers of (A) Pt cuboctahedra and (B) Pt octahedra.

packed 2-D phases were formed only for V_e < 350 Å, where short alkyl chain ligands were bound to the large particles. In our experiment, the chains of PVP are quite long, and they are likely entangled. The hydrophilic nature of the pyrrolidone ring in PVP also prevents the effective packing of particles through the hydrophobic interaction of long alkyl chain ligands.[19] The surface pressure increased suddenly when the Pt layer was further compressed. The monolayers started to collapse and form multilayer structures at the pressure of 10.6 mN/m (Figure 7D). Figure 7F shows the relationship between surface coverage and pressure of the particle layers. In the monolayer region, the coverage rapidly increases as the surface pressure increases.

The different shaped particles were deposited on the water surface in the same way. The PVP-capped cuboctahedral and octahedral particles were randomly distributed on the entire area of the TEM grids with tunable density (Figure 8). Even though close-packed 2-D structures were not generated here, high surface coverage of the Pt particles was obtained by increasing the surface pressure. It is interesting to mention the surface structure of the resulting layers. The {100} surfaces were enriched in the LB layer of Pt cubes (Figure 7), and the {111} faces were dominant in that of Pt octahedra. The surface of the cuboctahedra layer was in between. Therefore, we can adjust the surface structure of substrates by LB deposition using the different shapes of Pt nanocrystals.

Conclusions

We demonstrated that monodisperse Pt nanocrystals with various shapes including cubes, cuboctahedra, and octahedra can be synthesized selectively by a modified polyol process. The Ag ion plays a crucial role in controlling the shape and surface structure of the Pt nanocrystals. The resulting particles were deposited on the water surface to generate 2-D monolayers by the LB technique. The Pt coverage was controlled by changing the surface pressure, and the surface structure was modified by using different shapes of the particles.

Pt Nanocrystals: Shape and Surface Structure

J. Phys. Chem. B, Vol. 109, No. 1, 2005 **193**

The Pt nanocrystal monolayer can also be deposited on various metal oxide substrates such as silica and alumina by the same LB method. The resulting Pt nanocrystal/support structures are expected to be utilized as an ideal 2-D model catalyst as a result of their high surface area and the small/tunable interspacing between the particles compared to the lithography-based structures.[22] The ease of density control on the Pt layer is also beneficial for investigating the cooperative roles of metal particles and supports in such bifunctional catalysts. Studies on structure-dependent physical and chemical properties of the Pt particles and LB monolayers are in progress.

References and Notes

(1) (a) El-Sayed, M. A. *Acc. Chem. Res*. **2001**, *34*, 257. (b) Daniel, M.-C.; Astruc, D. *Chem. Rev*. **2004**, *104*, 293. (c) Kelly, K. L.; Coronado, E.; Zhao, L. L.; Schatz, G. C. *J. Phys. Chem. B* **2003**, *107*, 668. (d) Jin, R.; Cao, Y. C.; Hao, E.; Métraux, G. S.; Schatz, G. C.; Mirkin, C. A. *Nature* **2003**, *425*, 487. (e) Mock, J. J.; Barbic, M.; Smith, D. R.; Schultz, D. A.; Schultz, S. *J. Chem. Phys.* **2002**, *116*, 6755. (f) Puntes, V. F.; Krishnan, K. M.; Alivisatos, A. P. *Science* **2001**, *291*, 2115. (g) Dumestre, F.; Chaudret, B.; Amiens, C.; Renaud, P.; Fejes, P. *Science* **2004**, *303*, 821. (h) Somorjai, G. A.; Borodko, Y. G. *Catal. Lett.* **2001**, *76*, 1.

(2) (a) Murphy, C. J.; Jana, N. R. *Adv. Mater.* **2002**, *14*, 80. (b) Sun, Y.; Yin, Y.; Mayers, B. T.; Herricks, T.; Xia, Y. *Chem. Mater.* **2002**, *14*, 4736.

(3) (a) Kim, F.; Song, J. H.; Yang, P. *J. Am. Chem. Soc.* **2002**, *124*, 14316. (b) Yu, Y.-Y.; Chang, S.-S.; Lee, C.-L.; Wang, C. R. C. *J. Phys. Chem. B* **1997**, *101*, 6661.

(4) (a) Pastoriza-Sabtos, I.; Liz-Marzán, L. M. *Nano Lett.* **2002**, *2*, 903. (b) Chen, S.; Carroll, D. L. *Nano Lett.* **2002**, *2*, 1003.

(5) Sun, Y.; Xia, Y. *Science* **2002**, *298*, 2176.

(6) Kim, F.; Connor, S.; Song, H.; Kuykendall, T.; Yang, P. *Angew. Chem.*, *Int. Ed.* **2004**, *43*, 3673.

(7) Sau, T. K.; Murphy, C. J. *J. Am. Chem. Soc.* **2004**, *126*, 8648.

(8) (a) Ahmadi, T. S.; Wang, Z. L.; Green, T. C.; Henglein, A.; El-Sayed, M. A. *Science* **1996**, *272*, 1924. (b) Ahmadi, T. S.; Wang, Z. L.; Henglein, A.; El-Sayed, M. A. *Chem. Mater*. **1996**, *8*, 1161.

(9) (a) Chen, J.; Herricks, T.; Geissler, M.; Xia, Y. *J. Am. Chem. Soc.* **2004**, *126*, 10854. (b) Fu, X.; Wang, Y.; Wu, N.; Gui, L.; Tang, Y. *Langmuir* **2002**, *18*, 4619. (c) Zhao, S.-Y.; Chen, S.-H.; Wang, S.-Y.; Li, D.-G.; Ma, H.-Y. *Langmuir* **2002**, *18*, 3315. (d) Miyazaki, A.; Nakano, Y. *Langmuir* **2000**, *16*, 7109. (e) Teranishi, T.; Kurita, R.; Miyake, M. J. *Inorg. Organomet. Polym.* **2000**, *10*, 145.

(10) (a) Yoo, J. W.; Hathcock, D.; El-Sayed, M. A. *J. Phys. Chem. A* **2002**, *106*, 2049. (b) Balint, I.; Miyazaki, A.; Aika, K. *Chem. Commun.* **2002**, 1044. (c) Zhu, J.; Kónya, Z.; Puntes, V. F.; Kiricsi, I.; Miao, C. X.; Ager, J. W.; Alivisatos, A. P.; Somorjai, G. A. *Langmuir* **2003**, *19*, 4396. (d) Miyazaki, A.; Balint, I.; Nakano, Y. *J. Nanopart. Res.* **2003**, *5*, 69.

(11) Narayanan, R.; El-Sayed, M. A. *Nano Lett.* **2004**, *4*, 1343.

(12) Wang, Z. L. *J. Phys. Chem. B* **2000**, *104*, 1153.

(13) Somorjai, G. A. *Introduction to Surface Chemistry and Catalysis*; John Wiley & Sons: New York, 1994; Chapter 7.

(14) Petroski, J. M.; Wang, Z. L.; Green, T. C.; El-Sayed, M. A. *J. Phys. Chem. B* **1998**, *102*, 3316.

(15) (a) Zhang, Z.; Patel, R. C.; Kothari, R.; Johnson, C. P.; Friberg, S. E.; Aikens, P. A. *J. Phys. Chem. B* **2000**, *104*, 1176. (b) Petit, C.; Lixon, P.; Pileni, M.-P. *J. Phys. Chem.* **1993**, *97*, 12974. (c) Linnert, T.; Mulvaney, P.; Henglein, A.; Weller, H. *J. Am. Chem. Soc.* **1990**, *112*, 4657.

(16) Strüber, U.; Kastner, A.; Küppers, J. *Thin Solid Films* **1994**, *250*, 101.

(17) (a) Sun, Y.; Xia, Y. *J. Am. Chem. Soc.* **2004**, *126*, 3892. (b) Sun, Y.; Xia, Y. *Nano Lett.* **2003**, *3*, 1569.

(18) Yang, P. *Nature* **2003**, *425*, 243.

(19) (a) Markovich, G.; Collier, C. P.; Henrichs, S. E.; Remacle, F.; Levine, R. D.; Heath, J. R. *Acc. Chem. Res.* **1999**, *32*, 415. (b) Collier, C. P.; Saykally, R. J.; Shiang, J. J.; Henrichs, S. E.; Heath, J. R. *Science* **1997**, *277*, 1978. (c) Heath, J. R.; Knobler, C. M.; Leff, D. V. *J. Phys. Chem. B* **1997**, *101*, 189.

(20) Kim, F.; Kwan, S.; Akana, J.; Yang, P. *J. Am. Chem. Soc.* **2001**, *123*, 4360.

(21) (a) Tao, A.; Kim, F.; Hess, C.; Goldberger, J.; He, R.; Sun, Y.; Xia, Y.; Yang, P. *Nano Lett.* **2003**, *3*, 1229. (b) Whang, D.; Jin, S.; Wu, Y.; Lieber, C. M. *Nano Lett.* **2003**, *3*, 1255.

(22) (a) Zhu, J.; Somorjai, G. A. *Nano Lett.* **2001**, *1*, 8. (b) Eppler, A. S.; Zhu, J.; Anderson, E. A.; Somorjai, G. A. *Top. Catal.* **2000**, *13*, 33.